AIAA SciTech
5-9 January 2015, Kissimmee, Florida
53rd AIAA Aerospace Sciences Meeting

Reynolds–Averaged Navier–Stokes Simulations of Shock Buffet on Half Wing–Body Configuration

F. Sartor* and S. Timme†

University of Liverpool, Liverpool, England L63 3GH, United Kingdom

This paper presents a numerical study of transonic flow over a wing representative of a large transport aircraft. Reynolds–averaged Navier–Stokes simulations are conducted on a half wing-body configuration, with a Mach number close to cruise conditions and different angles of attack. The flow physics are discussed with particular attention to the separated zone induced by the shock wave. For small angles of attack, this zone is limited to the vicinity of the shock foot, and steady simulations converge. With increasing angle of attack, the separated region increases in size and begins to oscillate. This phenomenon, known as transonic shock buffet, is characterised by shock motions on the outboard section of the wing. In contrast to previous publications, three-dimensional shock buffet is reproduced by such unsteady simulation, and much information can be extracted analysing frequency content, location of unsteadiness and amplitude. The results provide an insight into the mechanism which is responsible for the onset of the unsteadiness.

I. Introduction

At cruise condition, the flow around the wing of a typical passenger aircraft is characterised by the presence of shock waves on the suction side of the profile. The result is the existence of high gradients, which are the shocks themselves and the shear layers resulting from the interaction with the boundary layers developing over a surface.[1] This can have a significant influence on the aircraft and often leads to undesirable effects such as loss of performance or structural damage.[2] Considering the flow over a wing, a strong interaction between the shock wave and the boundary layer may lead to significant separation. The consequence is the occurrence of large scale unsteadiness such as high-amplitude self-sustained shock movements, known as shock buffet, which arise for combinations of Mach number and angle of attack.[3] This phenomenon presents an industrial interest and has therefore been the subject of numerous studies in the past.

Shock buffet is a phenomenon that can be observed both in two- and three-dimensional configurations, from simple aerofoils to swept wings. In the particular two-dimensional case, the unsteadiness is characterised by self-sustained harmonic shock motions, occurring at a Strouhal number of about 0.2. The shock motions are often called low-frequency because they have much longer timescales than the unsteadiness associated with the separated zone or the turbulence structures in the boundary layer or wake. The phenomenon has been well documented in literature by means of experimental investigations[4,5,6] and numerical simulations.[7,8] Inviscid-viscous coupling approach has been able to predict the buffet onset with a fair accuracy,[9] while unsteady Reynolds–averaged Navier–Stokes (URANS) simulations have successfully reproduced the shock motions using various turbulence models.[10,11,12] More recently, high-fidelity approaches based on hybrid methods such as Zonal detached-eddy simulation (Zonal DES)[13] or URANS/large-eddy simulation (LES) coupling[14] have thoroughly described the physics of the flow trying to link the peak frequency describing the harmonic shock motions with a characteristic time scale of the interaction. From a more fundamental point of view, stability analysis has shown a strong link between the appearance of shock unsteadiness and the presence of an unstable global mode.[15,16] A critical value of the angle of attack exists above which the shock starts to oscillate and the onset can be described by a Hopf bifurcation.

*Research Associate, School of Engineering; fulvio.sartor@liverpool.ac.uk
†Lecturer, School of Engineering; sebastian.timme@liverpool.ac.uk

When considering more complex configurations, such as a wing representative of a large civil aircraft, the literature is more limited both for experiments and numerical investigations. Moreover, in this case the coupling between the flow unsteadiness and the structural response of the wing is an important factor that can lead to aeroelastic resonances, even more than when considering simple aerofoils. The unsteady behaviour presents some differences compared to the two-dimensional case[17] and the literature does not agree on the type of shock motions. Some authors have shown that the frequency spectrum has a distinct peak representative of shock oscillations, which are independent of the structural response of the wing.[18] Single-peaked spectra have also been observed on wings with small or zero sweep angle.[19] On the contrary, other studies indicate that in three-dimensional configurations the shock movements are broadband.[20,21] Looking at the time history of those signals, it can be argued that some periodic motions can always be found, and the large-band spectrum may be the result of numerical errors arising from a Fourier decomposition of a short signal. This disagreement on the frequency content of shock motions can also be found in wind tunnel tests. Some authors have reported very broadband spectra when measuring pressure fluctuations in the vicinity of the separated zone,[22] while some other studies have documented narrow peaks in the spectrum of shock location.[23] In experimental investigations of a flow over a half wing-body configuration, the pressure fluctuations can not be separated from the aeroelastic behaviour of the wind tunnel model due to the strong fluid-structure coupling.[24]

In the last decade, many numerical simulations have tried to describe the complex shock motions that characterise the three-dimensional buffet on a complete wing. Reynolds–averaged Navier–Stokes approaches indicated that the buffet onset can either be predicted by the presence of massive boundary layer separation[25] or by the pressure rise at the trailing edge.[26] Limited results have been produced by URANS approaches,[27] probably due to the high cost of these computations. Some authors have reproduced the shock unsteadiness using a Zonal DES approach and have argued that a URANS simulation is not adapted to reproduce the complex phenomenon of three-dimensional buffet.[28] A similar conclusion was drawn from the Aeroelastic Prediction Workshop,[29,30] where RANS models were shown to be insufficient for the correct physical modelling of the shock-induced vibration on a flexible wing. From a different perspective, shock motions occur at time scales that are much longer than those of the wall-bounded turbulence. Thus, a numerical simulation solving RANS equations closed with a turbulence model is justified. In this respect, recent studies have both presented the capability of URANS to simulate transonic tail buffet on a wing-body-tail model for a wide range of angles of attack[31] and reproduced the shock motions on simple three-dimensional configurations.[19]

This paper will discuss RANS and URANS simulations to analyse the flow around a half wing-body configuration at transonic speed. In particular the present investigation is focused on the buffet unsteadiness, its onset, and the flow condition that can cause the shock instability. The article proceeds in Section II with an introduction of the numerical approach and the configuration considered. Section III will present the main results of the steady-state solutions found by the RANS approach, while in Section IV we will discuss the time-dependent results obtained with time-accurate simulations. The unsteady features of the flow are presented in detail and compared with other studies. The conditions that determine the onset and the characteristics of the unsteadiness are discussed in Section V, where the available methods from literature for predicting the appearance of the instability are analysed. Section VI concludes the article by a summary of the major findings.

II. Numerical Approach

A. Flow Solver

The simulations were performed using the unstructured finite volume solver TAU, developed by the German Aerospace Center (DLR) and widely used in the European aerospace sector. The central scheme with scalar dissipation was used for the convective fluxes of the mean flow equations, while a first order Roe scheme was employed for the convective terms of the turbulence models. Gradients of the flow variables, used for the diffusive terms and source terms, are reconstructed using the Green-Gauss theorem. For the steady-state simulations a local time stepping and an implicit Backward Euler solver with an LU-SGS (Lower-Upper Symmetric Gauss-Seidel) scheme are used. For time accurate computations the standard dual time stepping approach is employed. Multigrid is not used in the current study.

Four turbulence models are considered, including the negative Spalart–Allmaras (SA),[32] the k–ω model with the Shear Stress Transport (SST) correction,[33] a Linearised Explicit Algebraic k–ω (LEA)[34] and an explicit algebraic Reynolds stress model in the form of Realizable Quadratic Eddy Viscosity Model (RQEVM).[34]

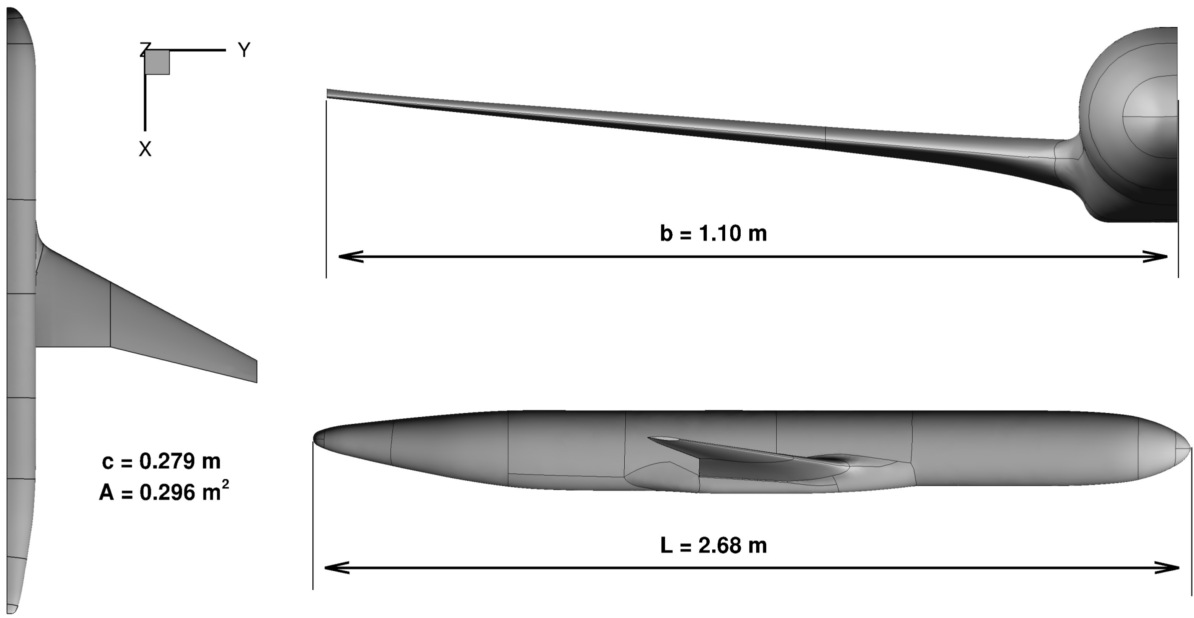

Figure 1. Top, front and side view of RBC12 half wing-body configuration.

While SA and SST models are widely discussed in literature and industry, the LEA model and RQEVM are not commonly implemented in production codes. The explicit algebraic Reynolds-stress models can be regarded as generalised two-parameter models, which retain the predictive benefits of the second-moment closure methodology, while numerical advantages of the Boussinesq-viscosity concept are conserved. The Reynolds stresses are modelled using up to a quadratic terms in the RQEVM, while the LEA model is the corresponding linear version. The main difference between the models is the prediction of the separated zone, which, as discussed in the next sections, plays a central role in the onset of the buffet instability. Where present, laminar regions close to the leading edge and nose of fuselage are obtained by limiting the turbulent production inside the boundary layers.

B. Test Case

The chosen test case is a half wing-body configuration, shown in figure 1, representative of a large transport aircraft. The model, referred to as RBC12, is a refurbishment of the B60 model studied in previous work to investigate the effect of nacelle installation on an aircraft wing.[35] The span of the model is 1.10 m, while the aerodynamic mean chord (AMC) is about 0.279 m. The local chord lengths corresponding to the centreline and wing tip are 0.592 m and 0.099 m, respectively. The wing is twisted, tapered and has a constant sweep angle of 25 deg. The trailing edge thickness of the aerofoil varies between 0.2 and 0.8 mm, depending on the span-wise location. Laminar to turbulent transition is imposed on the lower surface at about 5% of local chord, while on the upper surface this is at about 10% outboard of the crank and at 15% inboard.

The flow conditions are imposed to reproduce the aerodynamic field related to wind tunnel tests. The Mach number is 0.8 and the Reynolds number (based on the AMC) is 3.75 million. The reference temperature is 266.5 K and the reference pressure is 66 kPa. Far-field conditions are imposed at a distance corresponding to 25 times the span of the model (around 90 AMC). Symmetry boundary conditions were applied along the centre plane. For each turbulence model 24 configurations are considered, where the imposed angle of attack varies between 0.0 and 4.2 deg, with an increment of 0.1 deg close to onset conditions.

C. Grid

A family of three unstructured meshes produced using the Solar grid generator[36] is investigated. The coarsest mesh is composed of 2.7 million points (4.7 million elements), and a medium (8.1 million points, 17.4 million elements) and fine mesh (21.9 million points, 56.4 million elements) are also considered to assess the grid

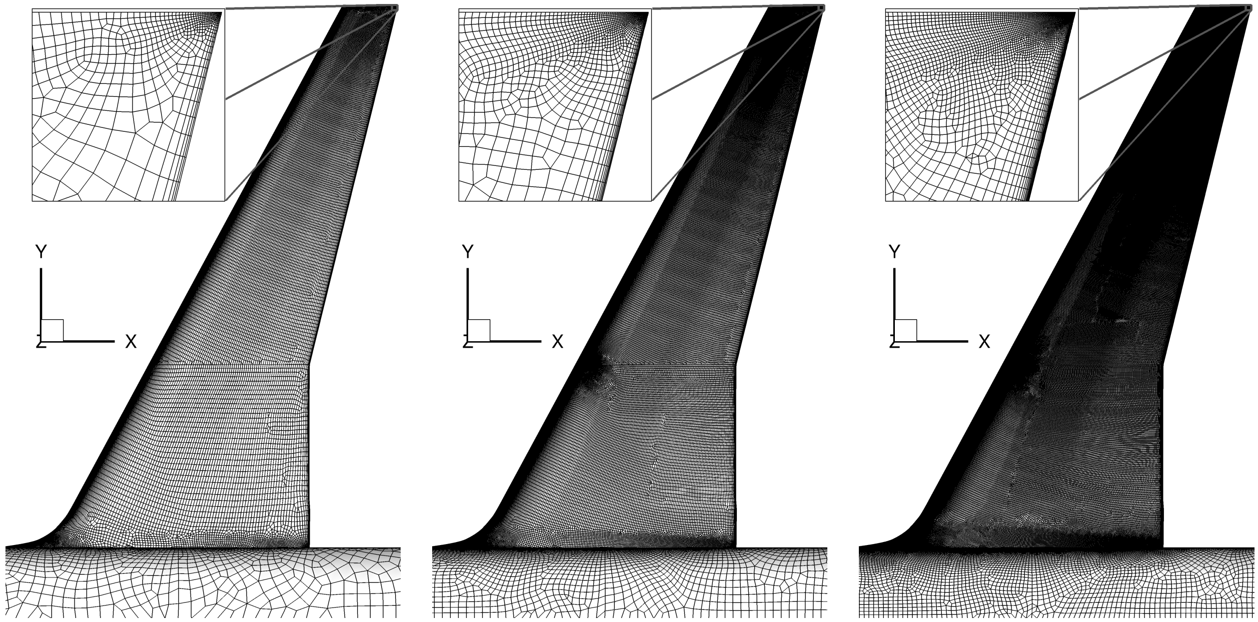

(a) Coarse (b) Medium (c) Fine

Figure 2. Mesh spacing on wing surface for family of grids.

resolution dependency. The grid spacing on the wing is presented in figure 2. The refinement approach is compatible with the strategy adopted in international workshops such as the Drag, High–Lift or Aeroelastic Prediction Workshop.[29]

The meshing also follows the industry accepted guidelines. For instance, the initial spacing normal to all viscous walls is less than $y^+ = 0.8$ for the coarse mesh, while the growth rate of cell sizes in the viscous layer is less than 1.3. The blunt trailing edge, which plays a central role in the buffet onset,[26] is described by 8 cells corresponding to a spacing of about 0.15% of the local chord. Concerning the span-wise mesh distribution, a spacing of 0.5% and 0.1% of the span is imposed for the wing root and tip, respectively. Altogether, the coarse grid consists of 12,000 prism, 71,000 pyramids, 2.4 million hexahedral and 2.3 million tetrahedral elements.

III. Steady-State Simulations

In this section we discuss the steady-state solutions. For each configuration, the RANS equations are solved using a Courant-Friedrichs-Lewy (CFL) number of 10. When considering finer grids and configurations at high angle of attack, an initialisation with a smaller CFL number and a first-order upwind scheme for the mean flow equations was needed. Multigrid acceleration is not used since a convergence study indicated that, for the considered meshes, the single-grid method was more efficient overall.

A. Grid Convergence and Turbulence Models

Figure 3 presents the steady-state solutions obtained with the three available grids using the SA and SST turbulence models. In figure 3a the evolution of the final density residual is plotted over the angle of attack. When the incidence is smaller than 3.0 deg, the results present a good level of convergence. After this threshold, the final residual rises and all cases fail to converge to the specified limit. The residuals reach a plateau and further iterations do not reduce their values. In those cases the steady-state results are not reliable and a URANS simulation should be considered instead to investigate the presence of unsteady flow features. Looking at the SST turbulence model, presented in figure 3b, a similar behaviour is observed.

Figure 3c presents the drag polar for the SA turbulence model. The grid dependency is limited, and different meshes predict the same forces even when the density residual indicated non-converged simulations. Figure 3d shows that for the SST turbulence model the mesh spacing dependency is limited only for the

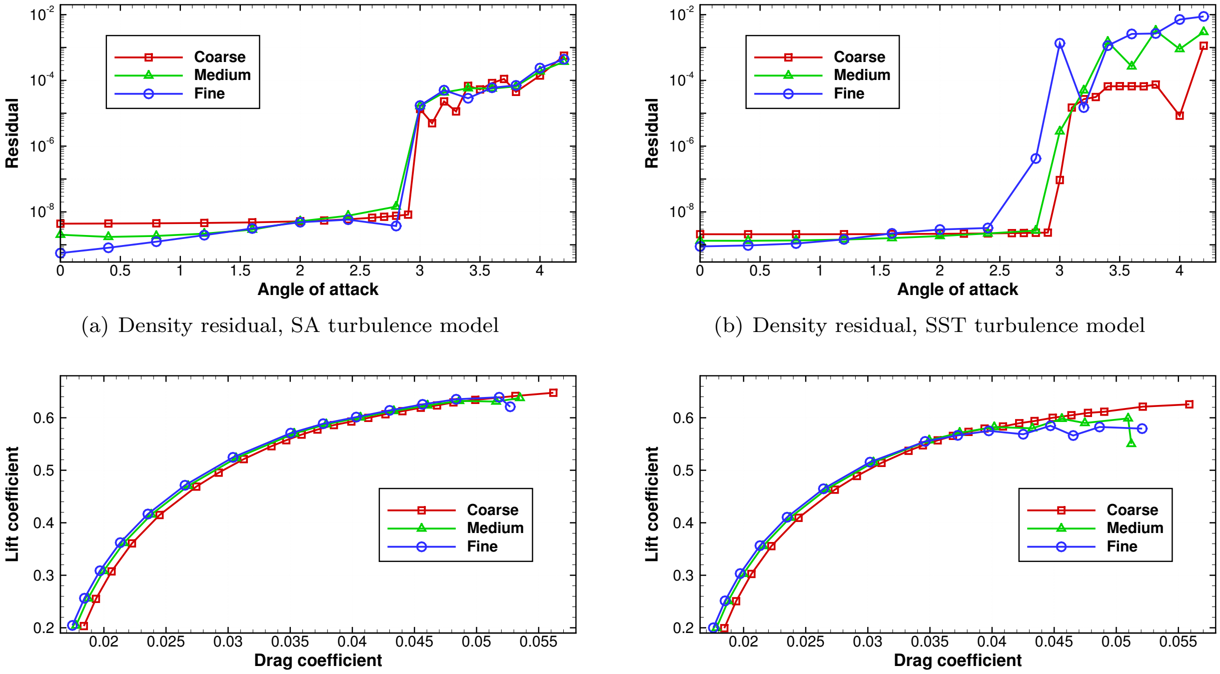

(a) Density residual, SA turbulence model

(b) Density residual, SST turbulence model

(c) Drag polar, SA turbulence model

(d) Drag polar, SST turbulence model

Figure 3. Steady-state solutions obtained using different grids.

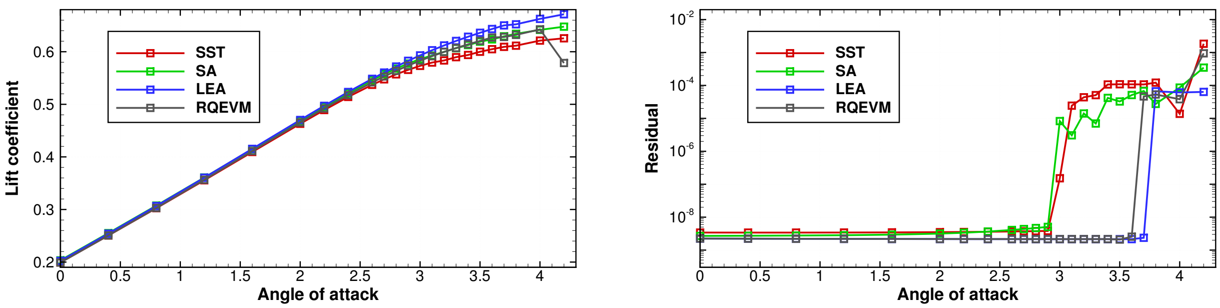

(a) Lift coefficient vs angle of attack

(b) Density residual vs angle of attack

Figure 4. Steady-state results obtained with different turbulence models using coarse grid.

cases where the angle of attack is small. Elsewhere, massive separated regions are not accurately predicted. Overall the mesh dependency is satisfying and the coarse grid is considered the remainder of the study.

In analogy with the grid-convergence study, the steady-state solutions obtained with different turbulence models at a given angle of attack are similar for small angles. As the angle of attack is increased, the separated zone on the wing becomes larger and is predicted by each turbulence model differently. The evolution of the lift coefficient with respect to the angle of attack is presented in figure 4a. A good agreement can be seen between SA and RQEVM (except for the highest angle of attack) while the SST model predicts the largest separation. For all cases, starting from 2.8 deg angle of attack, the lift coefficient is significantly diverging from its linear trend, suggesting that the shock-induced separation is drastically increasing.

As presented in figure 4b, a non-converged simulation towards steady state indicates the presence of a large separated zone, whereas a good convergence of the RANS equations suggests the absence of unsteady phenomena. This is the case for angles up to 2.8 deg where all turbulence models converge and a URANS simulation predicts steady flow as well. While producing a very similar lift coefficients, the SA model and RQEVM present different level of convergence for moderate angles of attack between 3.0 and 3.6 deg. This feature and its impact on the unsteady behaviour of the flow will be discussed in Section IV.

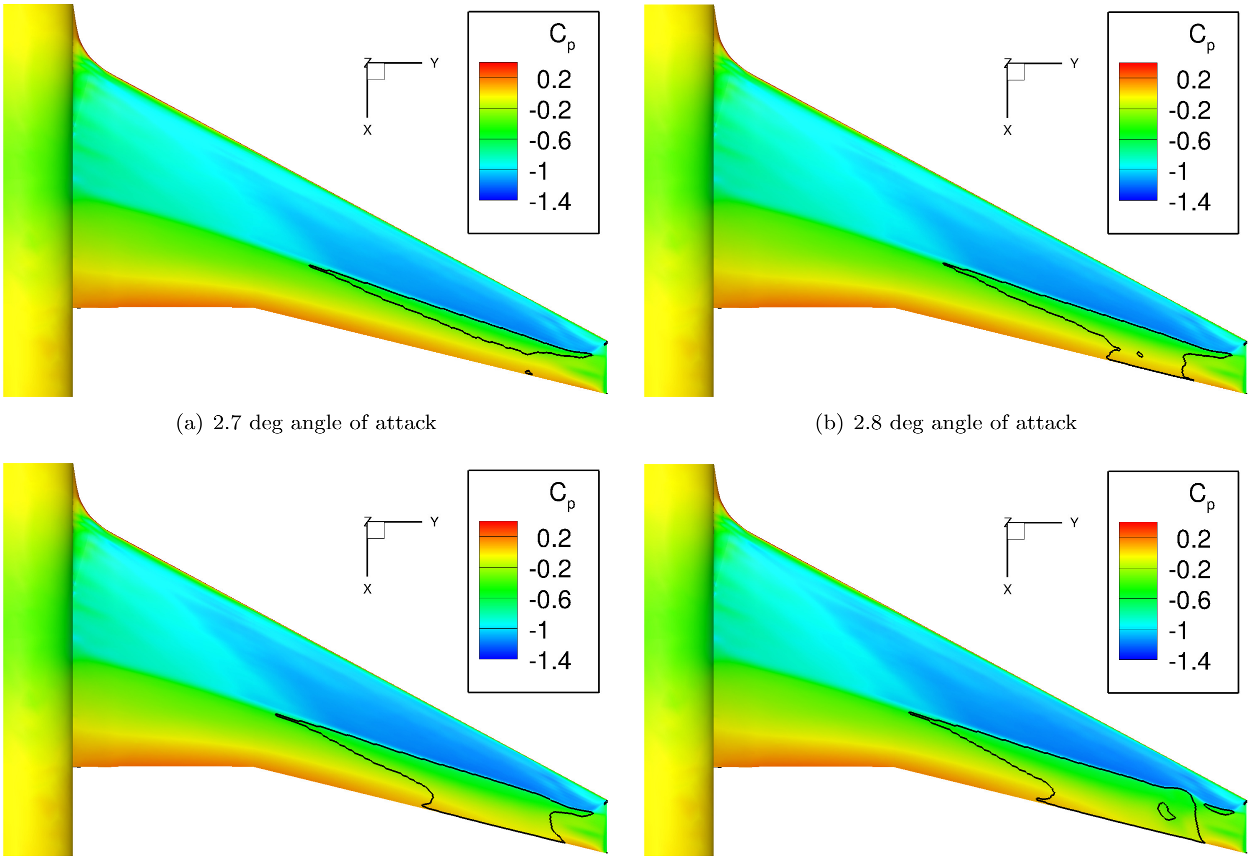

(a) 2.7 deg angle of attack

(b) 2.8 deg angle of attack

(c) 3.0 deg angle of attack

(d) Onset condition: 3.1 deg angle of attack

Figure 5. Surface pressure distribution and region of separation using SA turbulence model.

B. Discussion of Results for Buffet Onset

Despite the difference in the critical angle of attack that determines the appearance of massive separation and the onset of shock buffet, all the cases introduced so far present similar flow features. We focus now on the results obtained with the SA turbulence model, which will also be discussed in detail in Section IV when considering the URANS simulations.

A common method to predict the onset of unsteadiness is based on the presence of a large separated zone downstream of the shock foot. Although many studies in two-dimensional configurations do not show a clear link between buffeting flow and the topology of the flow separation,[15,16] the instability onset is often determined when the separated zone reaches the trailing edge and bursts.[25] Figure 5 presents the pressure distribution on the suction side of the wing for angles of attack just below and at buffet onset. In each plot, a solid black line is superposed where the skin friction coefficient changes sign, indicating the location of the separated zone. All configurations are compatible with the experimental results presented in Ref. [24]. On the inboard section of the wing, the local Mach number is relatively small and the pressure jump caused by the weak shock is smeared across the profile. When moving towards the wing tip, the pressure jump across the shock wave is more pronounced. The shock foot moves upstream on the wing surface with increasing angle of attack, and a shock-induced separation is then obtained when the local Mach number exceeds a given threshold.

In all cases presented in figure 5, when the angle of attack is small the separated zone is visible only outboard of the crank, and the reattachment line is on the wing surface. When increasing the angle of attack, the recirculation zone moves towards the trailing edge and increases in size. Eventually, as depicted in figure 5c for 3.0 deg angle of attack, the separated region in the wing tip vicinity extends from the shock foot to the trailing edge, where the recirculation zone is causing a pressure drop. A URANS simulation nevertheless indicates a steady flow. Shock buffet is observed once the angle of attack exceeds 3.1 deg, as

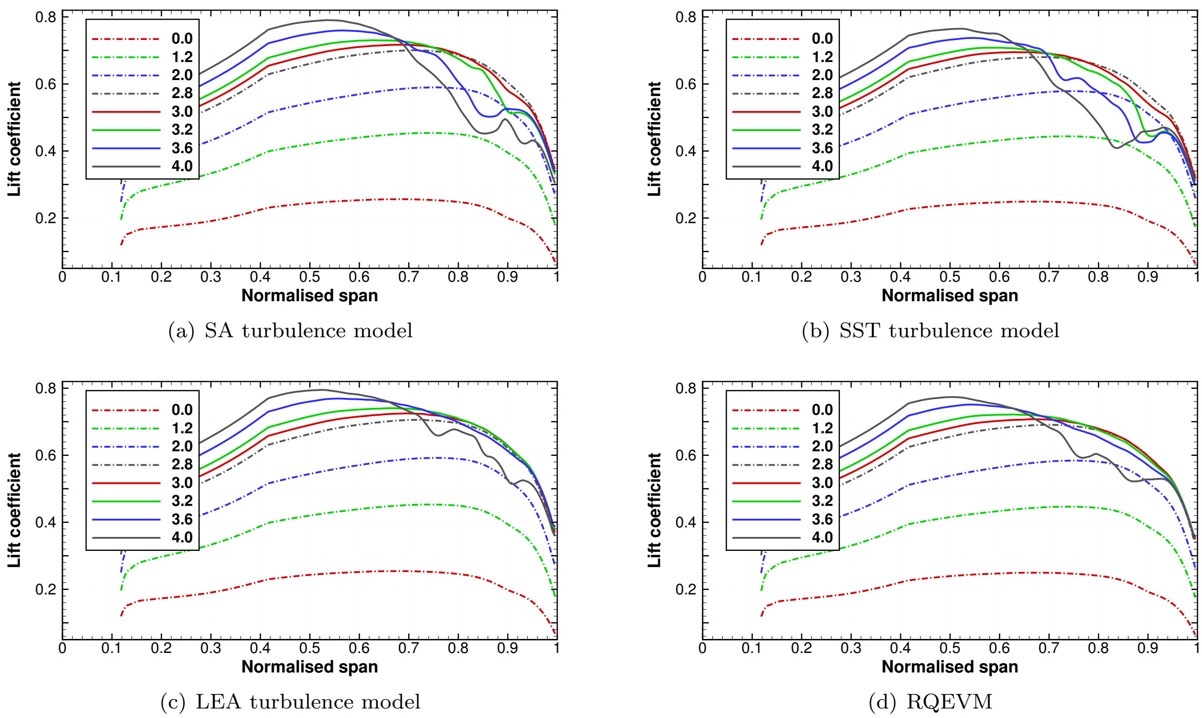

(a) SA turbulence model

(b) SST turbulence model

(c) LEA turbulence model

(d) RQEVM

Figure 6. Span-wise distribution of sectional lift coefficient for increasing angle of attack.

presented in figure 5d, where the separated zone is now split in different parts and most of it extends from the shock foot to the trailing edge.

Another common method to predict the presence of unsteadiness and its position is to analyse the distribution of the sectional lift coefficient along the span of the wing. For this purpose, the pressure coefficient of each steady-state solution is extracted along 200 wing sections and the lift coefficient is then computed considering the projection of the pressure coefficient in the direction normal to the free-stream direction. The result is presented in figure 6, showing the sectional lift from the wing root to the wing tip. The presence of the crank can be noticed by a small discontinuity at 42% of the span. Since the wing is twisted, the positive washout is responsible for the decreasing lift coefficient while approaching the wing tip. It is worth mentioning that for 2.0 deg angle of attack the highest lift-to-drag ratio is found using all turbulence models.

Inboard of the crank and in its vicinity, the sectional lift coefficients in figure 6 keep increasing constantly with the angle of attack. On the contrary, when focusing on the region close to the wing tip (at a span location greater than 70%), the increase in sectional lift is visible only up to 3.0 deg for the SA and SST turbulence model, and up to 3.6 deg for the LEA and RQEVM. Then the pressure loss due to the shock-induced separated zone causes an abrupt drop in the sectional lift coefficient. As previously noticed, the SST model predicts the largest separation, and thus the greatest pressure drop. A further increase in the angle of attack is responsible for a wider decrease of the sectional lift coefficient, indicating that the separation moves towards the fuselage. However, one should bare in mind that for those angles of attack the RANS simulation does not converge, indicating the requirement of an unsteady approach. Despite the disagreement on the angle of attack where large separations occur, results obtained with different turbulence models present a similar span-wise location of the separated zone, and a link can be found between the abrupt sectional-lift decrease and the appearance of unsteadiness.

IV. Unsteady Buffet Simulation

The RANS results described in the previous section are now used as a starting point for unsteady computations. The time discretisation is switched to dual-time stepping and every time step is iterated until a convergence criterion is reached. The total physical time simulated is 0.08 s for each case, corresponding

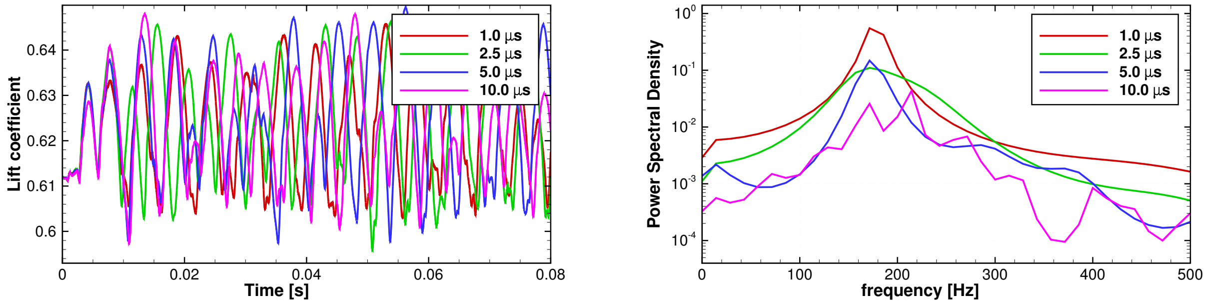

(a) Time history (b) Power spectral density

Figure 7. Time history and PSD of lift coefficients using different time steps and 100 inner iteration.

to 10–20 buffet cycles. In every simulation, a transient part can be observed, where the flow builds up the instability. Once the transient has passed, time histories of force and moment coefficients, as well as the mean and standard deviation of all flow variables are recorded. The power spectral density of the signals is then investigated in order to extract the frequency content of the unsteadiness.

A. Time Stepping and Grid Convergence

For an unsteady simulation, a time-step size has to be chosen appropriately depending on the time scale of the flow unsteadiness. A good measure is the convective time defined by the AMC and reference velocity, which for this case is around 10^{-3} s. The time step must be much smaller than this convective time, and a time-step study has to be considered to investigate the dependency of the solution to the temporal discretisation.[37] Thus, using the SST turbulence model and an angle of attack of 3.8 deg, a time-step convergence study has been performed for the coarse grid. The time-step sizes considered are 10 μs, 5 μs, 2.5 μs and 1 μs, which are between 100 to 1000 times smaller than the convective time. For each case, three simulations have been performed, where the number of inner iterations per physical time step was fixed to 25, 50 and 100. Results are only obtained when each buffet period is simulated with more than a certain number of total iterations. This can be achieved either with a small time-step size and fewer inner iterations, or with a bigger time step and more inner iterations. For instance, the computations converged with a time step of 2.5 μs and 25 inner iterations or with a time step of 10 μs and 100 inner iterations. The unsteady signals obtained, presented in figure 7a only for the case with 100 inner iteration per time step, have a similar mean value and amplitude, but different time history. During the initial transient, the time histories are similar but then quickly diverge from each other. It seems that the imperfect convergence in dual time at each real time step causes incremental solution differences to build up over a long unsteady signal. Further tests with 150, 200 and 250 inner iterations per real time step gave very similar results while shifting the point of divergence to the right.

The frequency content of the shock motions is now discussed by analysing the power spectral density (PSD) of the lift coefficient fluctuations obtained with different time steps and number of inner iterations, presented in figure 7b. As pointed out in Ref. [38], numerical signals issued from CFD are often oversampled and have a short duration. This can cause a problem since the spectrum definition is linked to the signal length. The solution adopted to overcome this problem is the use of an autoregressive estimator,[39] rather than a traditional Fast Fourier Transform. In particular, following the steps outlined in Ref. [13], the autoregressive PSD is computed using Burg's (or maximum entropy) method.[40] Each case is analysed using a single window covering the total duration of the lift signal without the initial transient. The order of the autoregressive model has been set to 2,000 after a parametric study.

When a solution is obtained, similar spectra can be observed when fixing the time step and changing the number of inner iterations. For all simulations, with the exception for the case with a time step of 10 μs, the dominant frequency is between 170 and 185 Hz. The time step required for physical modelling accuracy is thus smaller than 5 μs. Since the convergence study has been carried out for a particular configuration only, the time-step size chosen for all URANS simulations is 2 μs. This precaution has been taken to prevent inaccuracy in case the buffet frequency is significantly higher for some angle of attack. This value is almost three orders of magnitude smaller than the convective time.

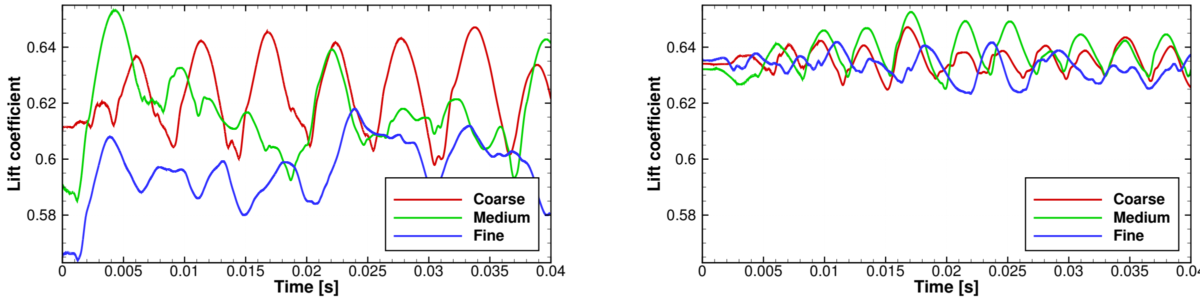

(a) SST turbulence model

(b) SA turbulence model

Figure 8. Histories of lift coefficients using different grids at 3.8 deg angle of attack.

Finally, it has to be considered that the shock-induced separated zone changes its size during a buffet cycle, depending on the shock position. Instead of performing a fixed number of iterations per time step, a Cauchy convergence criterion is applied. Hence, each time step is iterated until the drag coefficient in the last 20 inner iterations shows a relative error smaller than 10^{-8}. This criterion results in more inner iterations when in presence of a massive separation and fewer when the flow is easily converged. When the angle of attack is small, the separated zone has a limited extent and the flow converges quickly. In this case a minimum of 40 inner iterations per time step is performed. A maximum of 100 inner iterations per time step is imposed when the convergence criterion is not reached before.

As for the steady-state computations, the medium and fine meshes are here considered for grid convergence. If refinement in the spatial discretisation is introduced, the temporal discretisation should be adequately adjusted, since the fineness of the grid determines the flow features as much as the time scale.[37] For those reasons, the physical time step for the medium and fine grids are chosen to be 1.5 μs and 1 μs, respectively. The Cauchy criterion remains the same, while more inner iterations could be required to achieve the same convergence level. Thus, the maximal number of inner iterations is increased to 150 for the medium and to 200 for the fine grid.

Figure 8 shows histories of the lift coefficient at 3.8 deg angle of attack using the three meshes. For the SST turbulence model in figure 8a the lift predicted by the steady-state simulation differs significantly when comparing the three available grids. Then, after a small transient, the mean value of the lift coefficient for the coarse and medium grids are similar. The amplitude of oscillations obtained with the fine grid are 5% smaller than the others. Nevertheless, the frequency content of the unsteadiness seems to be similar among the considered cases. For the SA turbulence model, depicted in figure 8b, the lift coefficient presents a fairly smaller grid dependence. Both mean value and amplitudes of the unsteadiness are in good agreement, while the frequency content of the signals does not change when considering different mesh spacing.

B. Discussion of Time-Accurate Results

A wide range of angles of attack is now considered for each of the turbulence models introduced in Section III. The unsteady simulations are run for an initial period of 0.01 s, corresponding to the time needed for the buffet phenomenon to become fully developed. Then, the computations are continued until the signals reach 0.08 s, forces and moments are monitored, and the flow statistics are computed.

Figure 9 presents the time evolution of the lift coefficient, obtained with different turbulence models. It can be seen that 0.01 s are sufficient for the flow to established the fully developed shock buffeting regime, except for the LEA model and RQEVM at the maximum angle of attack considered. The lift coefficient does not diverge significantly from the steady-state simulations, with the exception of the RQEVM at 4.2 deg (figure 9d). This feature can be noticed in figure 4a, when comparing the lift coefficient predicted by the steady-state simulations. This is due to an overestimated separated region in the non-converged RANS simulation.

Figures 9a and 9b for the SST and SA turbulence models show an onset at 3.1 deg angle of attack. Comparing results at the same angle of attack, the SST model predicts more intense shock excursions compared to the SA model. The overall agreement is satisfying nevertheless. Not only do they predict the same onset, but for low angles of attack they also show periodic shock motions, in contrast to the LEA model

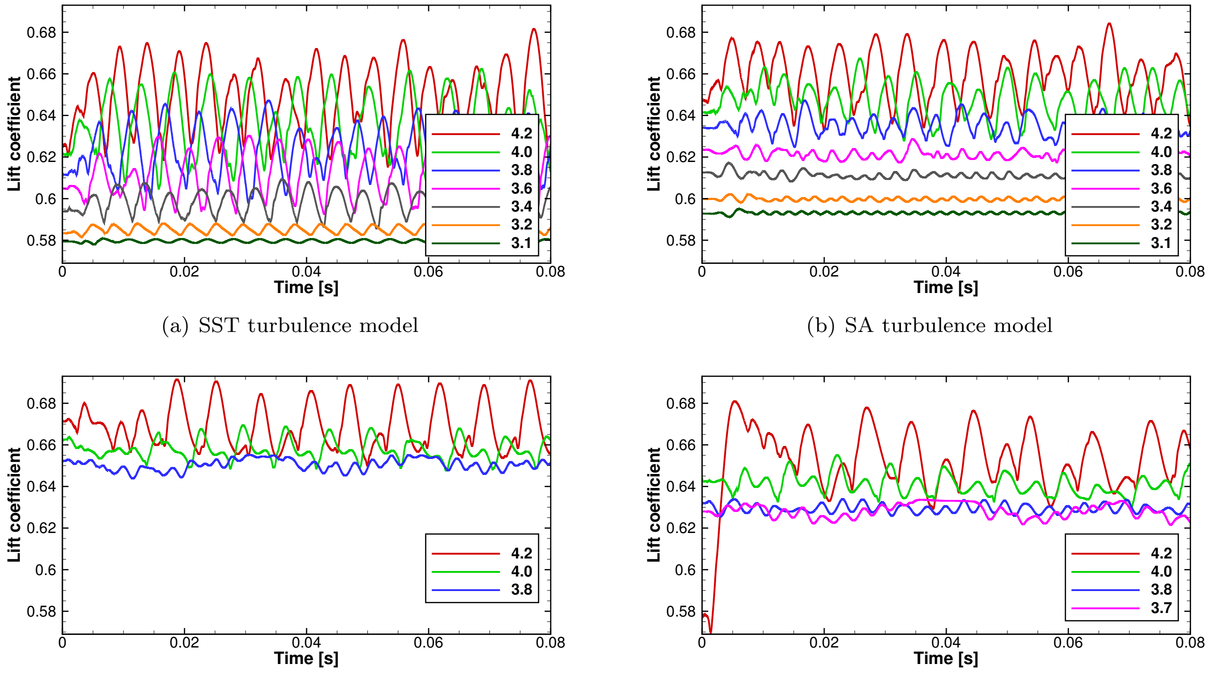

(a) SST turbulence model

(b) SA turbulence model

(c) LEA turbulence model

(d) RQEVM

Figure 9. Lift coefficients for angles of attack presenting shock oscillations using URANS simulations.

and RQEVM. This feature will be discussed in more detail below, when analysing the frequency content of the signals. Figures 9c and 9d were obtained with the LEA model and RQEVM. The two plots are similar to each other, yet different from those previously discussed. The buffet onset is now predicted at 3.8 deg and 3.7 deg for the LEA model and RQEVM, respectively. The signals are not periodic, not even at the onset conditions. However, when those two models predict unsteady shock motions, the lift coefficient compares favourably with those obtained with SST and SA models. In particular, as noticed in the steady-state simulations, a very good agreement can be observed between the SA turbulence model and RQEVM, both in terms of mean values and shock amplitudes.

During the unsteady simulations the standard deviation of the fluctuating velocity and pressure are computed. These quantities give access to the spatial distribution of the unsteady part of the flow. Figure 10 presents the pressure standard deviation σ_p, evaluated at the surface of the wing for four angles of attack and the SA turbulence model. The plot has a logarithmic scale colour map. In all cases the shock foot in the separated region is characterised by very high values of pressure fluctuations, up to 25% of the reference pressure. The rest of the separated region, where the bulk of the unsteadiness is located, presents standard-deviation values one order of magnitude smaller. This is true especially for small angles of attack, where both the recirculation region and the unsteady pressure zone have a limited extent (see for comparison figure 5). Then, the unsteady zones grows bigger and the centre of the unsteadiness moves towards the fuselage.

Figure 10a, showing the onset condition, is the only configuration where the unsteady zone is only limited to the separated zone. The unsteady shock trace lays on a straight line, roughly parallel to the the trailing edge. Then, from 3.2 deg angle of attack, presented in figure 10b, the shock is unsteady even where the flow does not separate, and its trace first bends in figure 10c and eventually adopts a serpentine shape in figure 10d. Figure 10c indicates that the whole shock foot is unsteady, regardless the presence of separation, even inboard of the crank. A very similar shock-foot trace has been observed in previous studies on a tapered and swept wing with a different plan form,[21] and on a non-tapered swept configuration.[19] Finally, high standard deviations indicate the presence of unsteady flow even on the leading edge, especially close to the wing tip. In figure 10d, for the highest angle of attack, the pressure is unsteady even on the fuselage.

The PSD results obtained as described when discussing the time-step convergence are presented for each turbulence model in figure 11. For the SST model in figure 11a, the onset condition occurs at 3.1 deg angle of attack with a very narrowband frequency, centred at 230 Hz. A first harmonic at 460 Hz is visible, but its

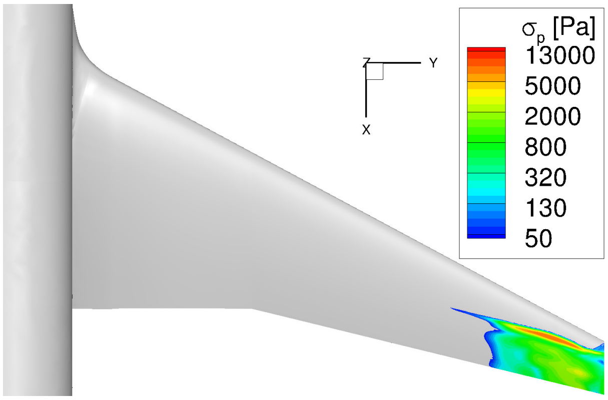

(a) Onset condition: 3.1 deg angle of attack

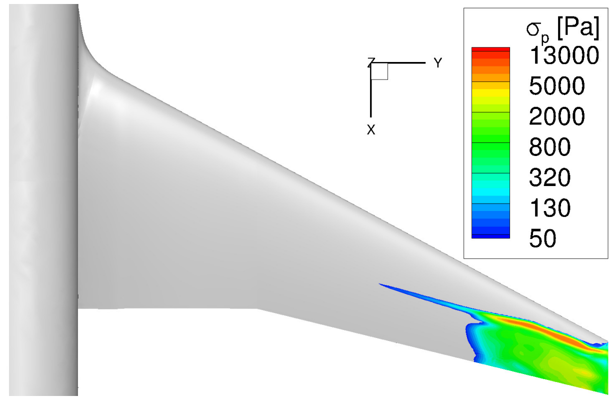

(b) 3.2 deg angle of attack

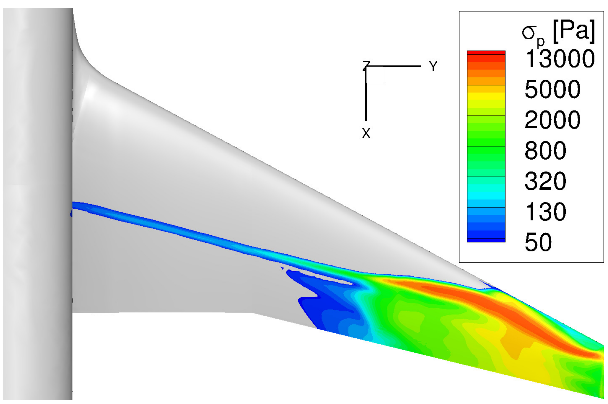

(c) 3.6 deg angle of attack

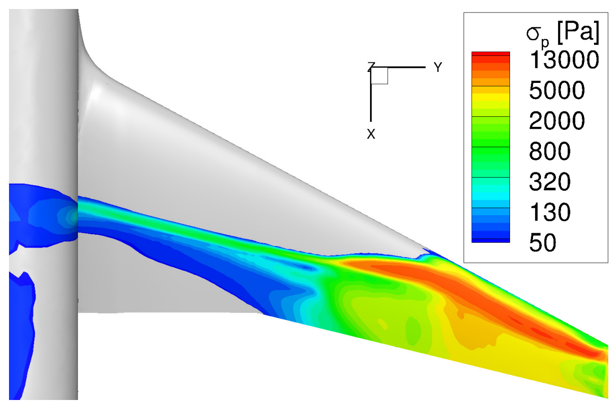

(d) 4.2 deg angle of attack

Figure 10. Standard deviation of pressure using the SA turbulence model.

energy is one order of magnitude smaller. However, at 3.2 deg angle of attack, the fundamental frequency and the first two harmonics present the same energy level, and their frequency remains almost unchanged from the case at 3.1 deg angle of attack. The presence of these periodic motions can be noticed also in figure 9a. When increasing the angle of attack, the lift signal presents greater shock motions and as a consequence the peak in the PSD is more energetic. A further increase in the angle of attack is responsible for this peak to move towards lower frequency and to become wider. The shock unsteadiness is now characterised by non-periodic motions.

A similar behaviour can be observed in figure 11b for the SA turbulence model. At the lowest angle of attack discussed, one single narrow peak is present. However, the spectrum indicates that the most energetic frequency is around 490 Hz, close to the first harmonic for the SST turbulence model. At 3.2 deg angle of attack, the PSD is similar to the SST turbulence model, with the first three peaks occurring at 220 Hz, 440 Hz and 660 Hz. As discussed before, those periodic motions can also be observed in figure 9b, and a further increase in the angle of attack is associated with a spectrum richer in frequency content. Figures 11c and 11d present the PSD obtained from results of the LEA model and RQEVM, respectively. In those cases the onset of the unsteadiness is associated with a single peak around 300 Hz, having a broader frequency content when compared to the two turbulence models discussed previously.

In conclusion the evolution of the lift coefficient at buffet onset conditions seems to be dominated by a narrowband frequency content. The lift signal predicted by the SA and SST turbulence models not only seems to be periodic, but is also characterised by a single-frequency harmonic motion. A similar result has been found in Ref. [18], who observed a distinct frequency in unsteady aeroelastic computations of a wing in transonic buffet conditions. Focusing on a configuration with 4.2 deg angle of attack, all turbulence models agree on shock motions occurring at a broadband peak whose frequency content is around 100 to 300 Hz. This corresponds, when scaled by a non-dimensional frequency given by the inverse of the convective time,

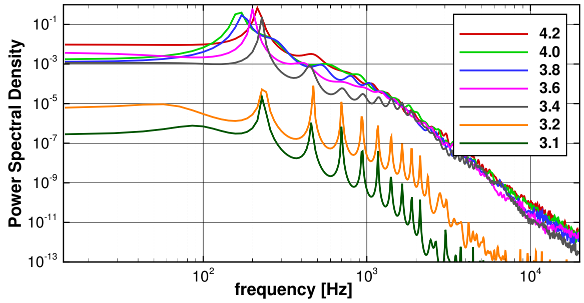

(a) SST turbulence model

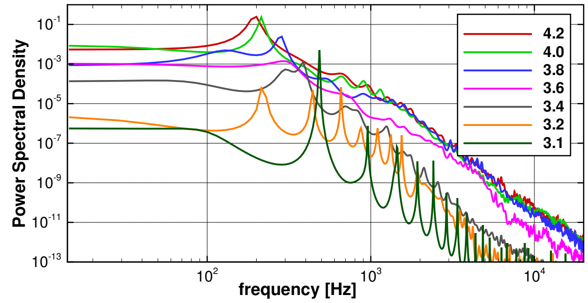

(b) SA turbulence model

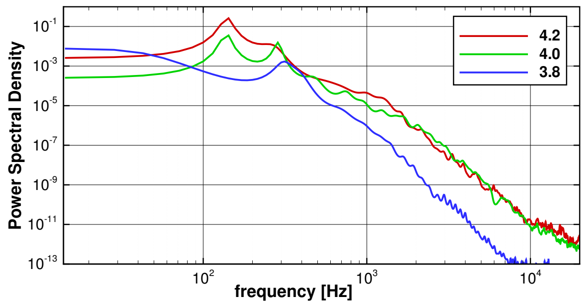

(c) LEA turbulence model

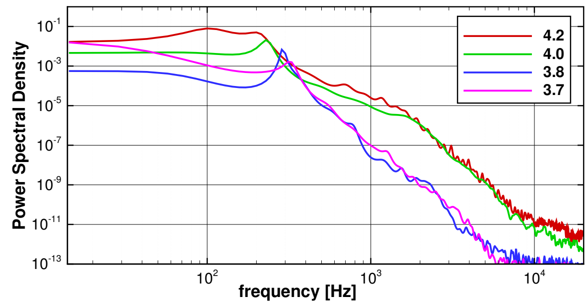

(d) RQEVM

Figure 11. Power Spectral Density of lift coefficient for various turbulence models.

to a Strouhal number of about 0.1 to 0.3. Overall, when focusing on angles of attack greater than 3.8 deg, all turbulence models predict transonic buffet, characterised by non-periodic shock motions. This observation is compatible with results obtained on a different configuration in Ref. [21] by means of Zonal DES. The signals observed in the current study are however less rich in high-frequency fluctuations, probably due to the lack of LES content in the URANS simulations.

V. Discussion on Buffet Mechanism

The high number of simulations considered in this study allows the creation of a database which, to the authors' knowledge, has not been documented in literature before. Previous studies were able to compare flow conditions at different angles of attack only for two-dimensional cases. More realistic studies on half-wing body configurations were limited to few angles of attack and often only one turbulence model. In this section we will discuss the major findings of the study and try to answer to some of the open questions concerning the buffet instability.

A. Prediction of Buffet Onset Using Steady Results

The results presented indicate that the shock motions in transonic flow around a wing-body configuration can be described by URANS simulations. While high-fidelity approaches can improve the quality of the results, the URANS approach is sufficient to describe the buffet phenomenon. However, even if less expensive than higher-fidelity scale-resolving approaches, time-accurate simulations remain infeasible in a production environment. Much effort has been invested in the past to predict the onset of the instability using steady-state solutions.[26,41]

In this respect, Ref. [42] showed experimentally that the distinct slope change (or kink) in the lift curve coincides with buffet onset as measured with a strain gauge on a two-dimensional aerofoil. When extending this concept to the three-dimensional case, the link between lift coefficient predicted by the steady state solutions and the unsteady behaviour of the separated zone is not straightforward. On the one hand, the lift versus angle of attack curves presented in figure 4a clearly show a divergence to the linear trend when the angle of attack is close to onset conditions. On the other hand, we observed a strong disagreement between the results stemming from the unsteady simulations for the SA model and RQEVM in figures 9b and 9d. While the onset of the buffet instability is at 3.1 deg and 3.8 deg angle of attack, respectively, the two lift curves depicted in figure 4a present the same trend. Thus, the simplified model would predict the same onset. Other similar methods based on the presence of a kink in the lift vs moment curves have been applied to a three dimensional case[43] and have shown that buffet onset is accompanied by a sudden change in the wing loads. This feature was not encountered in this study since the variation of forces and moments are smooth for all the angles of attack considered.

Discussing the flow around a profile, Ref. [25] affirmed that buffet onset is determined by the Mach number or incidence when the separated zone reaches the trailing edge and bursts. A more general picture was given in Ref. [44], where the onset boundary was defined as a curve separating the attached and partially separated regions from those totally separated. Considering a three-dimensional case, the comparison between figures 5 and 9b indicate that this method is not reliable. Even though the separated zone extends from the shock foot to the trailing edge for angles of attack greater than 2.8 deg, unsteady motions are only observed beyond 3.1 deg. A similar behaviour is found for all turbulence models.

The latter method corresponds to the current results better than the first. The presence of a massively separated zone can easily be noticed also form the sectional lift distribution presented in figure 6. The abrupt drop in the sectional lift coefficient indicates that the separated zone induced by the shock has merged with the separated zone at the trailing edge. In addition, this method can give an idea of the location of the unsteady phenomenon, even if the link between steady state and unsteady result is not assured. In fact, the RANS results predicting a massive separation often fail to converge, and hence the simulation should not be trusted without considering a time-accurate simulation.

B. Characteristics of Flow Instability Using Unsteady Data

When considering unsteady simulations, much information on the buffet instability can be obtained. In particular, the results presented in the previous section have shown some important features observed for all considered case. First, the unsteady motions start at the wing tip and move towards the fuselage with increasing angle of attack. Secondly, the shock motions have a frequency content that becomes more broadband when increasing the angle of attack, and the most energetic frequency in the PSD decreases when increasing the incidence. The consequence of those two phenomena is that the buffet onset is characterised by shock motions significantly different from those observed when the instability is fully developed.

A common method used in literature to explain the shock oscillation frequency in a buffeting flow has been provided in Ref. [45]. According to this method, the separation point generates a disturbance that propagates downstream and interacts with the trailing edge of the aerofoil. The pressure waves generated by this interaction then propagate upstream to the shock to feed the generation of the downstream-travelling instability. In the proposed model, the period of the shock oscillation is proportional to the time needed by a disturbance to propagate from the shock to the trailing edge and then back to the shock.

In the two-dimensional case the distance between the mean shock location and the trailing edge remains roughly constant when increasing the incidence of the profile. Thus, following the model of Ref. [45], the main frequency of the buffet remains constant. When considering the flow over a wing however, this feature is not observed. The frequency of the unsteadiness changes with the angle of attack. This behaviour can be explained by the observation that the shock unsteadiness moves towards the inner part of the wing, as presented in figure 10, where the chord is longer because of the tapered wing plan. As a consequence, the distance between the shock-foot mean position and the trailing edge increases as the angle of attack is increased. The time needed for a perturbation to complete the buffet cycle is thus higher, giving a lower frequency of unsteadiness.

The decrease of the main frequency is associated to a widening of the peak describing the shock motions, as depicted by the PSD in figure 11. When increasing the angle of attack, shock motions occur in a larger span-wise section of the wing involving a wider range of chord lengths. Then, the phenomenon can neither be considered two-dimensional nor the unsteadiness periodical. In addition, once the unsteadiness is fully developed, as shown in figure 10, the distance between the mean shock location and the leading edge is not constant in the span-wise direction. This concept is in agreement with results obtained on an infinite-swept configuration,[19] where a two-dimensional nature of the buffet is observed when considering wings with small sweep angles. Because of the symmetry of the wing and the shock-induced separation, the buffet instability mechanism remains similar to the two-dimensional case, which is characterised mainly by chord-wise shock oscillations.

Concerning the onset of the instability, the turbulence models considered do not agree on the topology of the shock motions. The first two turbulence models predicted periodic oscillations characterised by a single frequency, whilst the others indicated aperiodic motions. It can be argued that the onset of the instability appears in a critical section of the wing. If a turbulence model predicts the buffet onset when the span-wise extent of the separated zone is limited, the phenomenon can be considered two-dimensional and periodic motions are observed. This is not the case for the LEA model and RQEVM, where the onset of the instability occurs when the separation already covers a large part of the wing. Following again the model presented in Ref. [45], the time needed for a perturbation to travel from the shock foot to the trailing edge and then back will depend on the span-wise location of the perturbation. Since for those two models a wide range of chord lengths are involved even at onset condition, the buffet period is not characterised by a single peak, but by a broadband frequency content.

VI. Conclusions

The flow over a typical large transport aircraft at cruise conditions was analysed considering a half wing-body model. It has been shown that steady-state solutions can give solid results only when the flow does not present a large separated zone on the upper surface of the wing. Then, unsteady simulations have to be considered. After spatial and temporal convergence have been assessed, the results clearly indicate that URANS simulations are capable to predict, within the general limitations of RANS modelling, the main features of the flow. When varying the angle of attack, all the considered turbulence models can give information about the stationary shock-wave/boundary-layer interaction on the wing, the onset of buffet unsteadiness, and the unsteady shock motions occurring in a transonic flow over a swept wing. The results discussed present a step forward in the simulation of three-dimensional flow around a civil aircraft at cruise conditions by means of a RANS approach.

When considering small angles of attack, the shock-induced separation has a limited size and the flow is steady. Increasing the incidence, the separated zone close to the wing tip begins to oscillate. The shock motions seem to be periodic, similarly to the unsteadiness found in two-dimensional aerofoils. However, as demonstrated by the power spectral density of the unsteady lift coefficient, the frequency content is often not limited to a single harmonic fluctuation. Overall, the mechanism responsible for the unsteadiness at onset conditions remains similar to its two-dimensional nature. This feature, never observed in previous studies, revealed a link between the results in two-dimensional cases and in more realistic configurations. Once the instability is fully developed, the lift-coefficient fluctuations have greater amplitudes and their temporal behaviour is not limited to periodic oscillations. The unsteady separated zone extends from the wing tip to the crank and shock motions affect the whole wing. The power spectral density of the lift fluctuations indicate that shock motions occur between 100 and 300 Hz and the main frequency content shift to lower frequency values when increasing the angle of attack. This value is within the range of what is typically reported for transonic buffet. A link between the wing sections where buffet occurs and its frequency has been proposed.

In the current study, a single Mach number was considered representative of the flow at cruise conditions. However, the flight envelope often presents more than one Mach number, and thus it will be interesting to consider the same half wing-body configuration at different speeds. A future study will address the influence of the free-stream Mach number in order to investigate how the buffet phenomenon in general, and the onset in particular, are impacted by the change in the incoming flow properties.

Acknowledgments

The authors wish to acknowledge Simon Lawson from Aircraft Research Association for the inspection of the RBC12 model and for providing the meshes. The research leading to these results has received funding from the European Union's Seventh Framework Programme (FP7/2007-2013) for the Clean Sky Joint Technology Initiative under grant agreement n° 336948. Part of this work made use of the facilities of N8 HPC provided and funded by the N8 consortium and EPSRC (Grant n° EP/K000225/1).

References

[1]Dolling, D. S., "Fifty years of shock-wave/boundary-layer interaction research: what next?" *AIAA Journal*, Vol. 39, No. 8, 2001, pp. 1517–1531.

[2]Délery, J. and Marvin, J. G., "Shock-wave boundary layer interactions," *AGARDograph No. 280*, 1986.

[3]Lee, B. H. K., "Self-sustained shock oscillations on airfoils at transonic speeds," *Progress in Aerospace Sciences*, Vol. 37, No. 2, 2001, pp. 147–196.

[4]McDevitt, J. B., Levy, J. L. L., and Deiwert, G. S., "Transonic flow about a thick circular-arc airfoil," *AIAA Journal*, Vol. 14, No. 5, 1976, pp. 606–613.

[5]McDevitt, J. B. and Okuno, A. F., "Static and dynamic pressure measurements on a NACA 0012 airfoil in the Ames high Reynolds number facility," *NASA TP-2485*, 1985.

[6]Jacquin, L., Molton, P., Deck, S., Maury, B., and Soulevant, D., "Experimental study of shock oscillation over a transonic supercritical profile," *AIAA Journal*, Vol. 47, No. 9, 2009, pp. 1985–1994.

[7]Brunet, V., "Computational study of buffet phenomenon with URANS equations," *AIAA Paper 2003–3679*, 2003.

[8]Iovnovich, M. and Raveh, D. E., "Reynolds-averaged Navier-Stokes study of the shock-buffet instability mechanism," *AIAA Journal*, Vol. 50, No. 4, 2012, pp. 880–890.

[9]Edwards, J. W., "Transonic shock oscillations with a new boundary layer coupling method," *AIAA Paper 93–0777*, 1993.

[10]Barakos, G. and Drikakis, D., "Numerical simulation of transonic buffet flows using various turbulence closures," *International Journal of Heat and Fluid Flow*, Vol. 21, No. 5, 2000, pp. 620–626.

[11]Goncalves, E. and Houdeville, R., "Turbulence model and numerical scheme assessment for buffet computations," *International journal for numerical methods in fluids*, Vol. 46, No. 11, 2004, pp. 1127–1152.

[12]Thiery, M. and Coustols, E., "Numerical prediction of shock induced oscillations over a 2D airfoil: Influence of turbulence modelling and test section walls," *International Journal of Heat and Fluid Flow*, Vol. 27, No. 4, 2006, pp. 661–670.

[13]Deck, S., "Numerical simulation of transonic buffet over the OAT15A airfoil," *AIAA Journal*, Vol. 43, No. 7, 2005, pp. 1556–1566.

[14]Garnier, E. and Deck, S., "Large-eddy simulation of transonic buffet over a supercritical airfoil," *Turbulence and Interactions*, Springer, 2010, pp. 135–141.

[15]Crouch, J. D., Garbaruk, A., Magidov, D., and Travin, A., "Origin of transonic buffet on aerofoils," *Journal of Fluid Mechanics*, Vol. 628, 2009, pp. 357–369.

[16]Sartor, F., Mettot, C., and Sipp, D., "Stability, receptivity and sensitivity analyses of buffeting transonic flow over a profile," *Accepted for publication to AIAA Journal*, 2014.

[17]Benoit, B. and Legrain, I., "Buffeting prediction for transport aircraft applications based on unsteady pressure measurements," *AIAA Paper 87–2356*, 1987.

[18]Farhangnia, M., Guruswamy, G. P., and Biringen, S., "Transonic-buffet associated aeroelasticity of a supercritical wing," *AIAA Paper 96–0286*, 1996.

[19]Iovnovich, M. and Raveh, D. E., "Numerical Study of Shock Buffet on Three-Dimensional Wings," *AIAA Journal*, 2014, pp. 1–15.

[20]Reneaux, J., Brunet, V., Caruana, D., Deck, S., and Naudin, P., "A combined experimental and numerical investigation of the buffet phenomenon and its control through passive and active devices." *ONERA Tiré à Part*, Vol. 2005, No. 103, 2005.

[21]Brunet, V. and Deck, S., "Zonal-detached eddy simulation of transonic buffet on a civil aircraft type configuration," *Advances in Hybrid RANS-LES Modelling*, Springer, 2008, pp. 182–191.

[22]Molton, P., Dandois, J., Lepage, A., Brunet, V., and Bur, R., "Control of Buffet Phenomenon on a Transonic Swept Wing," *AIAA Journal*, Vol. 51, No. 4, 2013, pp. 761–772.

[23]Caruana, D., Mignosi, A., Corrègeand, M., Pourhiet, A. L., and Rodde, A. M., "Buffet and buffeting control in transonic flow," *Aerospace science and technology*, Vol. 9, No. 7, 2005, pp. 605–616.

[24]Steimle, P. C., Karhoff, D.-C., and Schröder, W., "Unsteady Transonic Flow over a Transport-Type Swept Wing," *AIAA Journal*, Vol. 50, No. 2, 2012, pp. 399–415.

[25]Pearcey, H. H., "A method for the prediction of the onset of buffeting and other separation effects from wind tunnel tests on rigid models," Tech. rep., DTIC Document, 1958.

[26]Rumsey, C. L., Allison, D. O., Biedron, R. T., Buning, P. G., Gainer, T. G., Morrison, J. H., Rivers, S. M., Mysko, S. J., and Witkowski, D. P., "CFD sensitivity analysis of a modern civil transport near buffet-onset conditions," *NASA TM-2001-211263*, 2001.

[27]Rumsey, C. L., Morrison, J. H., and Biedron, R. T., "CFD Variability for a Civil Transport Aircraft Near Buffet-Onset Conditions," *NASA TM-2003-212149*, 2003.

[28]Brunet, V. and Deck, S., "Zonal-detached eddy simulation of transonic buffet on a civil aircraft type configuration," *AIAA Paper 2008–4152*, 2008.

[29]Heeg, J., Chwalowski, P., Florance, J. P., Wieseman, C. D., Schuster, D. M., and Perry, B., "Overview of the Aeroelastic Prediction Workshop," *AIAA Journal*, Vol. 783, 2013, pp. 7–10.

[30]Dalenbring, M., Jirasek, A., Heeg, J., and Chwalowski, P., "Initial Investigation of the Benchmark SuperCritical Wing Configuration using Hybrid RANS-LES modeling," *AIAA Paper 2013–1799*, 2013.

[31]Illi, S. A., Fingskes, C., Lutz, T., and Krämer, E., "Transonic Tail Buffet Simulations for the Common Research Model," *AIAA Paper 2013–2510*, 2013.

[32]Allmaras, S. R. and Johnson, F. T., "Modifications and clarifications for the implementation of the Spalart-Allmaras turbulence model," *ICCFD7-1902, 7th International Conference on Computational Fluid Dynamics, Big Island, Hawaii*, 2012.

[33]Menter, F. R., "Two-equation eddy-viscosity turbulence models for engineering applications," *AIAA Journal*, Vol. 32, No. 8, 1994, pp. 1598–1605.

[34]Rung, T., Lübcke, H., Franke, M., Xue, L., Thiele, F., and Fu, S., "Assessment of explicit algebraic stress models in transonic flows," *Engineering turbulence modelling and experiments 4*, 1999, pp. 659–668.

[35]Peiró, J., Peraire, J., Morgan, K., Hassan, O., and Birch, N., "The Numerical Simulation of Flow about Installed Aero-Engine Nacelles Using a Finite Element Euler Solver on Unstructured Meshes," *Aeronautical Journal*, , No. 96-956, 1992.

[36]Martineau, D. G., Stokes, S., Munday, S. J., Jackson, A. P., Gribben, B. J., and Verhoeven, N., "Anisotropic hybrid mesh generation for industrial RANS applications," *AIAA Paper 2006-534*, 2006.

[37]Cummings, R. M., Morton, S. A., and McDaniel, D. R., "Experiences in accurately predicting time-dependent flows," *Progress in Aerospace Sciences*, Vol. 44, No. 4, 2008, pp. 241–257.

[38]Deck, S. and Nguyen, A. T., "Unsteady side loads in a thrust-optimized contour nozzle at hysteresis regime," *AIAA Journal*, Vol. 42, No. 9, 2004, pp. 1878–1888.

[39]Kay, S. M. and Marple, S. L. J., "Spectrum analysis – a modern perspective," *Proceedings of the IEEE*, Vol. 69, No. 11, 1981, pp. 1380–1419.

[40]Burg, J. P., "Maximum entropy spectral analysis," *Modern Spectrum Analysis*, Edited by D. G. Childers, IEEE Press, New York, 1978, pp. 34–41.

[41]Chung, I., Lee, D., Reu, T., and Ko, D., "Prediction of transonic buffet onset for airfoils with separation bubble using steady approaches," *Journal of Aircraft*, Vol. 40, No. 4, 2003, pp. 795–797.

[42]Pearcey, H. H. and Holder, D. W., "Simple methods for the prediction of wing buffeting resulting from bubble type separation," *Aero Rep. 1024*, 1962.

[43]Gariépy, M., Malouin, B., Trépanier, J.-Y., and Laurendeau, É., "Far-Field Drag Decomposition Applied to the Drag Prediction Workshop 5 Cases," *Journal of Aircraft*, Vol. 50, No. 6, 2013, pp. 1822–1831.

[44]Thomas, F. and Redeker, G., *A method for calculating the transonic buffet boundary including the influence of Reynolds number*, DFVLR, 1971.

[45]Lee, B. H. K., "Oscillatory shock motion caused by transonic shock boundary-layer interaction," *AIAA Journal*, Vol. 28, No. 5, 1990, pp. 942–944.